Journal of Computational Mathematics, Vol.22, No.4, 2004, 622–632.

KINETIC FLUX VECTOR SPLITTING FOR THE EULER EQUATIONS WITH GENERAL PRESSURE LAWS *1)

Hua-zhong Tang
(*LMAM, School of Mathematical Sciences, Peking University, Beijing 100871, China*)

Abstract

This paper attempts to develop kinetic flux vector splitting (KFVS) for the Euler equations with general pressure laws. It is well known that the gas distribution function for the local equilibrium state plays an important role in the construction of the gas–kinetic schemes. To recover the Euler equations with a general equation of state (EOS), a new local equilibrium distribution is introduced with two parameters of temperature approximation decided uniquely by macroscopic variables. Utilizing the well-known connection that the Euler equations of motion are the moments of the Boltzmann equation whenever the velocity distribution function is a local equilibrium state, a class of high resolution MUSCL–type KFVS schemes are presented to approximate the Euler equations of gas dynamics with a general EOS. The schemes are finally applied to several test problems for a general EOS. In comparison with the exact solutions, our schemes give correct location and more accurate resolution of discontinuities. The extension of our idea to multidimensional case is natural.

Mathematics subject classification: 65M06,76M20, 76N15.
Key Words: KFVS method, The Euler equations, General equation of state.

1. Introduction

The development of KFVS schemes and BGK–type schemes for compressible flow simulations has attracted much attention and becomes mature in the past few years. The gas-kinetic schemes have provided robust and accurate numerical solutions for various unsteady compressible flows (see [3, 11, 13, 14, 15, 16, 17, 18, 20]).

Numerical simulation of compressible flows of real gases has been conducted by several authors in [5, 6, 7, 8, 9, 12, 22]. Colella and Glaz in [5] obtained an exact Riemann solver for real gases. Glaister in [7] presented an approximate linearised Riemann solver for the Euler equations with a general EOS. Grossman and Walters [8], and Liou, van Leer and Shuen [9], Vinokur and Montagne [22] extended flux–vector splitting and flux–difference splitting to the Euler equations with general pressure laws.

Most of the previous methods would require a computation of the pressure law and its derivatives, or a Riemann solver. This is costly and problematic when there is no analytic expressions of the pressure law. Recently Coquel and Perthame [6] introduced an energy relaxation theory for the Euler equations of real gas. Their method does not need computations of derivatives of the pressure law or a Riemann solver. In [12], Montarnal and Shu studied the implementation of this relaxation method with high order WENO schemes for real gases.

As we know, the gas distribution function for a local equilibrium state plays an important role in the construction of gas-kinetic schemes, and the Maxwellian distribution function, or

* Received April 10, 2002; Final revised March 30, 2003.
1) This research was supported partly by the special Funds for Major State Basic Research Projects of China (No. G1999032801-14), the National Natural Science Foundation of China, and the Alexander von Humboldt foundation.

the Maxwell-Boltzmann distribution can be used to recover the Euler equations with a γ–gas law. However, one cannot use these equilibrium distribution functions to recover the Euler equations with a general EOS. In order to do it, a new equilibrium distribution with two parameters of temperature approximation will be introduced in this paper to recover the Euler equations with general pressure laws. These parameters can be decided uniquely by macroscopic variables. Moreover, using the well-known connection that the Euler equations of motion are the moments of the Boltzmann equation whenever the velocity distribution function is a local equilibrium state, we will also give a class of high resolution KFVS methods to approximate the Euler equations of gas dynamics with a general EOS. They do not depend on the particular expression of the equation of state, besides without derivatives of the pressure law or any Riemann solvers. Finally, several test problems for some special EOSs will be solved by the present schemes to show their performance.

The paper is organized as follows. In next section we will recall the connection between the Boltzmann and the Euler equations, and introduce a new equilibrium distribution function to recover the Euler equations with a general EOS, which can be considered as a generalized local Maxwellian distribution function. In Section 3, a class of high resolution KFVS schemes are presented based on the local equilibrium distribution function introduced in Section 2, and the van Leer's interpolation method. In Section 4, we give several numerical experiments on a standard shock reflection test problem and two shock-tube problems for three different EOSs to show the performance of the current schemes. We conclude the paper with a few remarks in section 5.

2. A New Local Equilibrium Distribution

The Euler equations governing inviscid compressible fluid flows can be described as equations for the mass, momentum and energy densities, $\rho(x,t)$, $\rho(x,t)u(x,t)$, and $E = \frac{1}{2}\rho u^2 + \rho e(x,t)$, i.e.

$$\frac{\partial U}{\partial t} + \frac{\partial F(U)}{\partial x} = 0, \tag{2.1}$$

where

$$U = [\rho,\ \rho u,\ E]^T, \quad F(U) = \left[\rho u, \rho u^2 + p, u(E+p)\right]^T. \tag{2.2}$$

In the above ρ, u, p, and e represent the density, velocity, pressure, and the specific internal energy density, respectively.

The system (2.1) is not complete. We should consider an additional equation, i.e. the EOS, which is a macroscopic thermodynamic relationship specific to each particular fluid, and assume here that it can be written in the form

$$p = p(\rho, e). \tag{2.3}$$

Moreover, the function $p(\cdot,\cdot)$ will be assumed to satisfy conditions which ensure that the system (2.1) is hyperbolic. In the case of an ideal gas, (2.3) becomes

$$p = (\gamma - 1)\rho e, \tag{2.4}$$

here γ is the ratio of specific heat capacities of the fluid.

Flow motion can also be described from viewpoint of particle motion, or the statistical description of a fluid. Due to the large number of particles in small volume in common situations, to follow each one is impossible. Instead, a continuous distribution function $f(x_i, t, v_i)$ is used to describe the probability of particles to be located in a certain velocity interval, and to approximate usually the particle number density at a certain velocity in hydrodynamics. The velocity distribution function f is a basic unknown in the kinetic theory of gases, and obeys a particle conservation law, known as the Boltzmann equation, which is given by

$$\frac{\partial f}{\partial t} + v \cdot \frac{\partial f}{\partial x} = J(f, f), \tag{2.5}$$

where the right hand side term of the above equation represents a molecular collision term, which vanishes in the Euler limit.

The thermodynamic aspect of hydrodynamical equations is based on the assumption that the departure of the gas from local equilibrium state is sufficiently small. The real gas distribution function f usually is unknown in the real flow situation, but in classical physics we know the distribution function g corresponding equilibrium state locally if the mass, momentum and energy densities are known. The gas distribution function for equilibrium state plays an important role in studying some physical properties in fluid and the construction of gas-kinetic schemes, see [3, 11, 13, 14, 15, 16, 17, 18, 20]. Here we omit understanding its physical properties and refer the reader to [2, 4] for details. Moreover, for convenience, we will mainly limit our attention to one dimensional case.

For compressible Euler equations (2.1) with a γ–gas law (2.4), if defining Maxwell-Boltzmann distributions for the equilibrium state

$$g = \rho(\frac{\lambda}{\pi})^{\frac{1+K}{2}} e^{-\lambda[(v-u)^2+\xi^2]}, \tag{2.6}$$

then the Euler equations can be cast in the moment form as

$$\left\langle \Psi, \frac{\partial g}{\partial t} + v \cdot \frac{\partial g}{\partial x} \right\rangle = 0,$$

where K is the internal degree of freedom, $K = -1 + 2/(\gamma - 1)$, λ is a function of the density and pressure, $\rho = 2\lambda p$, $\xi^2 = \xi_1^2 + \cdots + \xi_K^2$, and the moment $< \Psi, g >$ is defined as

$$< \Psi, g >= \int_{R\times R^K} \Psi g \; d\Xi,$$

with $d\Xi = dv d\xi_1 \cdots d\xi_K$. Here the moment function vector Ψ is given by

$$\Psi = \left[1, \; v, \; \frac{v^2+\xi^2}{2}\right]^T.$$

Unfortunately, when we consider a general EOS (2.3), the Euler equations (2.1) cannot be written in the moment form through the Maxwell-Boltzmann distribution g. To overcome this difficulty, we modify the distribution g defined in (2.6) as follows

$$\bar{g} = \rho(\frac{\lambda_1}{\pi})^{\frac{1}{2}}(\frac{\lambda_2}{\pi})^{\frac{K}{2}} e^{-\lambda_1(v-u)^2-\lambda_2\xi^2}, \tag{2.7}$$

where λ_1 and λ_2 are two new functions of temperature, molecule mass and Boltzmann constant, and are decided below.

For a local equilibrium state with $f = \bar{g}$, taking moments of Ψ to Eq. (2.5), we can obtain the conservative variables and corresponding flux as

$$\begin{pmatrix} \rho \\ \rho u \\ \frac{1}{2}(\rho u^2 + \frac{\rho}{2\lambda_1} + K\frac{\rho}{2\lambda_2}) \end{pmatrix} = \int_{R\times R^K} \Psi \; \bar{g} \; d\Xi, \tag{2.8}$$

and

$$\begin{pmatrix} \rho u \\ \rho u^2 + \frac{\rho}{2\lambda_1} \\ \frac{1}{2}u(\rho u^2 + 3\frac{\rho}{2\lambda_1} + K\frac{\rho}{2\lambda_2}) \end{pmatrix} = \int_{R\times R^K} v \; \Psi \; \bar{g} \; d\Xi. \tag{2.9}$$

Comparing equation (2.8) and (2.9) to (2.1), we show if λ_1 and λ_2 satisfy the following representations

$$\frac{\rho}{2\lambda_1} = p, \quad e = \frac{1}{4\lambda_1} + \frac{K}{4\lambda_2}, \tag{2.10}$$

then the Euler equations (2.1) with a general EOS (2.3) can be recovered by the distribution function $\bar{g}$, i.e.

$$\left\langle \Psi, \frac{\partial \bar{g}}{\partial t} + v \cdot \frac{\partial \bar{g}}{\partial x} \right\rangle = 0. \tag{2.11}$$

Remark. (a) It is also physically reasonable to construct two temperature approximation in $\bar{g}$, because non-ideal gas means that the random transport and internal energy do not reach equal-partition, the so-called same amount of energy for each degree of freedom. (b) For (2.4), it is not difficult to find that $\lambda_2 = \lambda_1$ as well as $\bar{g} = g$. (c) For the general EOS (2.3) and numerical purpose, assuming that three conservative variables ρ, ρu, and E are known, we solve equation (2.3) for the pressure p by some approximate methods, for example Newton's iterative method. Then parameters λ_1 and λ_2 can be decided from (2.10), i.e. $\lambda_1 = \rho/2p$, and $\lambda_2 = \rho K/4(\rho e - \frac{1}{2}p(\rho, e))$. (d) Actually, the parameters λ_1 and λ_2 should be nonnegative such as the parameter λ in Eq.(2.6). It is a essential prerequisite to ensure that the moment $< \Psi, \bar{g} >$ is finite. That is to say, the specific internal energy density e may be decomposed into two nonnegative parts, see Eq.(2.10). We also refer the reader to Fig.12.

3. High Resolution KFVS Schemes

Following the idea in [3, 11, 14, 17], we develop a class of flux vector splitting algorithm for the Euler equations for real gases based on (2.11) and (2.7) in this section.

Let $x_j = j\Delta x (j \in Z)$ be an uniform meshes and Δx the mesh size in x–direction. The cell averaged conservative variables are denoted by

$$U_j = \frac{1}{\Delta x} \int_{x_{j-1/2}}^{x_{j+1/2}} U(x,t)\, dx.$$

Depending on the sign of the molecular velocity, we can split the macroscopic flux $F(U)$ into two parts, a positive flux and a negative flux, such as

$$F(U) = F^+(U) + F^-(U) = \int_{R^K} \int_0^{+\infty} v\Psi\bar{g}\, d\Xi + \int_{R^K} \int_{-\infty}^0 v\Psi\bar{g}\, d\Xi. \tag{3.1}$$

Based on this, it is easy to derive a first order accurate KFVS difference scheme

$$U_j^{n+1} = U_j^n - \frac{\Delta t}{\Delta x}(G(U_j^n, U_{j+1}^n) - G(U_{j-1}^n, U_j^n)), \tag{3.2}$$

to approximate the Euler equations (2.1) with the general EOS (2.3), where the numerical flux $G(U_j^n, U_{j+1}^n)$ at the cell interface $j + 1/2$ is defined by

$$G(U_j^n, U_{j+1}^n) = F^+(U_j^n) + F^-(U_{j+1}^n). \tag{3.3}$$

The positive and negative fluxes can be given in an explicit form

$$F^{\pm}(U) = \begin{pmatrix} \rho < v^1 >_{\pm} \\ \rho < v^2 >_{\pm} \\ \frac{1}{2}\rho \left(< v^3 >_{\pm} + < v^1 >_{\pm} < \xi^2 > \right) \end{pmatrix}$$

where

$$\rho < \cdots >= \int \int_{-\infty}^{+\infty} (\cdots)\bar{g}\, dvd\xi, \quad \rho < \cdots >_{\pm} = \pm \int \int_0^{\pm\infty} (\cdots)\bar{g}\, dvd\xi.$$

These moments can be computed as follows

$$< \xi^2 >= \frac{K}{2\lambda_2},$$
$$< v^0 >_{\pm}= \frac{1}{2}\mathrm{erfc}(\mp\sqrt{\lambda_1}u),$$
$$< v^1 >_{\pm}= u < v^0 >_{\pm} \pm\frac{1}{2}\frac{e^{-\lambda_1 u^2}}{\sqrt{\pi\lambda_1}},$$
$$\cdots\cdots$$
$$< v^{n+2} >_{\pm}= u < v^{n+1} >_{\pm} + \frac{n+1}{2\lambda_1} < v^n >_{\pm},$$

where the complementary error function $\mathrm{erfc}(x)$ has been used, which is generally a given function in FORTRAN.

The first order accurate scheme (3.3) is very dissipative. In order to reduce the numerical dissipation, an initial reconstruction technique[21] can be used to interpolate the cell averaged conservative variables.

For simplicity, a linear function

$$\bar{U}_j^n(x) = U_j^n + S_j^n(x - x_j), \quad \text{for } x \in [x_{j-1/2}, x_{j+1/2}] \tag{3.4}$$

is used to approximate the cell averaged conservative variables U_j at each time level $t = t_n$, where S_j is an approximate slope at the grid point x_j,

$$S_j^n = \frac{\partial}{\partial x}U(x_j, t_n) + O\big((\Delta x)^p\big), \quad p \geq 1.$$

Using a simple polynomial expansion leads usually to generate spurious overshoot and undershoot, or even oscillations if large variations in data are present initially. The most reliable interpolation techniques is to combine any nonlinear limiter with polynomial expansion. For example, a discrete form of the slope of U together with van Leer's limiter[21] is

$$S_j^n = (\mathrm{sgn}(s_j^+) + \mathrm{sgn}(s_j^-))\frac{\mid s_j^+ \mid\mid s_j^- \mid}{\mid s_j^+ \mid + \mid s_j^- \mid}, \tag{3.5}$$

where

$$s_j^+ = (U_{j+1}^n - U_j^n)/(x_{j+1} - x_j), \; s_j^- = (U_j^n - U_{j-1}^n)/(x_j - x_{j-1}).$$

Combining the other expansions with different form of nonlinear limiter can also be considered. Based on the linear reconstruction (3.4) and (3.5), a class of high resolution MUSCL-type KFVS schemes can be obtained

$$U_j^{n+1} = U_j^n - \frac{\Delta t}{\Delta x}(G(\bar{U}_j^+, \bar{U}_{j+1}^-) - G(\bar{U}_{j-1}^+, \bar{U}_j^-)), \tag{3.6}$$

where

$$\bar{U}_j^+ = U_j^n + \frac{\Delta x}{2}S_j^n, \quad \bar{U}_j^- = U_j^n - \frac{\Delta x}{2}S_j^n,$$

and the numerical flux $G(U, V)$ is defined by (3.3).

Remark. The above KFVS finite volume schemes (3.2) and (3.6) do not depend on the particular expression of the EOS, besides without derivatives of the pressure law or a Riemann solver.

4. Numerical Results

In this section we present some numerical experiments to demonstrate the performance of the MUSCL-type KFVS schemes (3.4)–(3.6) for the Euler equations with a general EOS, including the correctness and robustness.

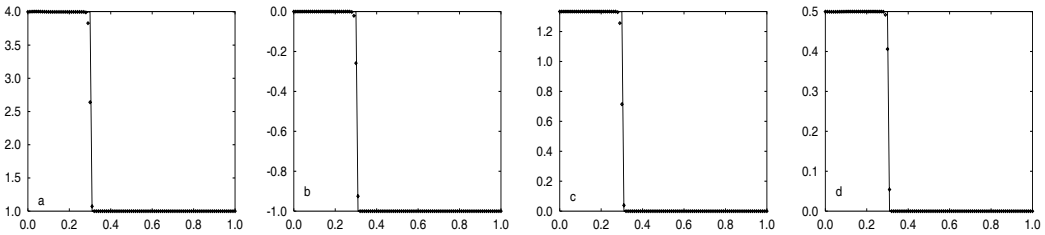

Figure 1: A shock reflection problem for (2.4) with $\gamma = 5/3$ and the pressure ratio $p^+/p^- \approx \infty$. The solutions at $t = 0.9$ are obtained by with 100 points and $\Delta t = 0.003$. (a) Density. (b) Velocity. (c) Pressure. (d) Internal energy.

We will mainly use the following three different forms of equation of state for a fluid, the ideal gas-law (2.4), a stiffened EOS and a general EOS:

$$p = B(\frac{\rho}{\rho_0} - 1) + (\gamma - 1)\rho e, \tag{4.1}$$

$$p = \frac{1}{\rho_0 e + \psi_0} \left\{ \zeta(a_1 + a_2|\zeta|) + \rho_0 e[b_0 + \zeta(b_1 + b_2\zeta) + \rho_0 e(c_0 + c_1\zeta)] \right\}, \tag{4.2}$$

where B is a constant, ρ_0 represents a reference density, $\zeta = \rho/\rho_0 - 1$, and constants ρ_0, a_1, a_2, b_0,b_1, b_2, c_0, c_1, and ψ_0 depend on the material in question.

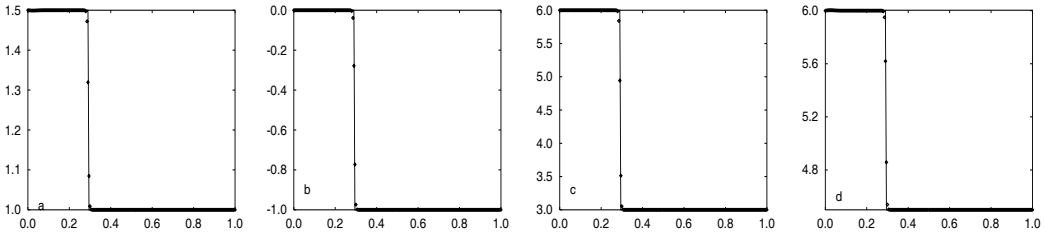

Figure 2: Same as Figure 1, except with the pressure ratio $p^+/p^- = 2$, $\Delta t = 0.0026$, 200 grid cells, and $t = 0.145$.

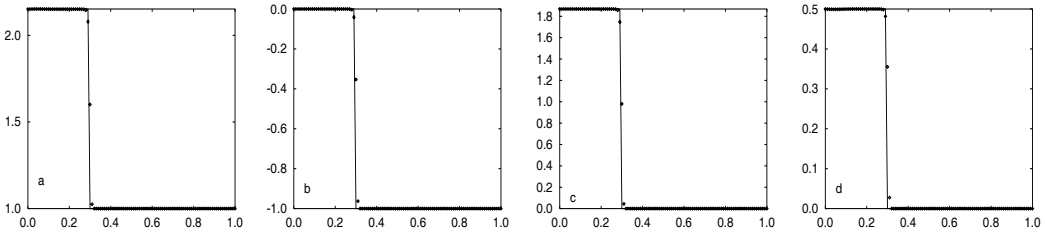

Figure 3: A shock reflection problem for stiffened EOS (4.1) with $\gamma = 5/3$ and the pressure ratio $p^+/p^- \approx \infty$. The solutions at $t = 0.344$ are obtained with 100 points and $\Delta t = 0.002$. (a) Density. (b) Velocity. (c) Pressure. (d) Internal energy.

The first problem we consider is concerned with shock reflection in one dimension for three EOS listed above. The initial condition is set in a computational domain $0 \le x \le 1$ as

$$\rho = \rho_0, \quad u = -u_0, \quad e = e_0, \quad p = p(\rho_0, e_0).$$

The boundary $x = 0$ is a rigid wall, at where the gas is brought to rest and the flow variables take post–shocked values given by the Rankine–Hugoniot shock relations. The exact solution describes shock reflection from the wall. Here uniform grids and 5/3 for γ are used in all cases.

Each of Figs. 1–6 refers to one of the equations of state with different values of the initial conditions and parameters. The solid lines denote the exact solution, and the dashed lines are numerical solutions. For the ideal and stiffened one, we take $\rho_0 = 1$, $u_0 = 1$, and $B = 1.0$. For the general equation of state (4.2), we take

$$\begin{aligned} &\rho_0 = 8.9, && a_1 = 4.9578, && a_2 = 3.6884, \\ &b_0 = 7.4727, && b_1 = 11.519, && b_2 = 5.5251, \\ &c_0 = 0.39493, && c_1 = 0.52883, && \psi_0 = 3.6, \end{aligned}$$

and $u_0 = 1$. For all ones, the pressure jump across the shock takes the two values ∞, and 2.

From Figs. 1–6, we observe that strong shocks are resolved very well on the uniform grid and the results are comparable to other scheme in [7] and the exact solutions (the solid lines). In this problem, p^+ and p^- have been used to represent the post-shocked pressure value and pre-shocked pressure value, respectively.

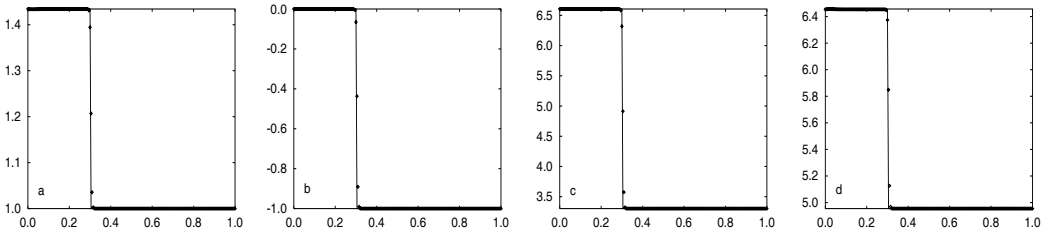

Figure 4: Same as Figure 3, except for the pressure ratio $p^+/p^- = 2$, $\Delta t = 0.0011$, 200 grid cells, and $t = 0.132$.

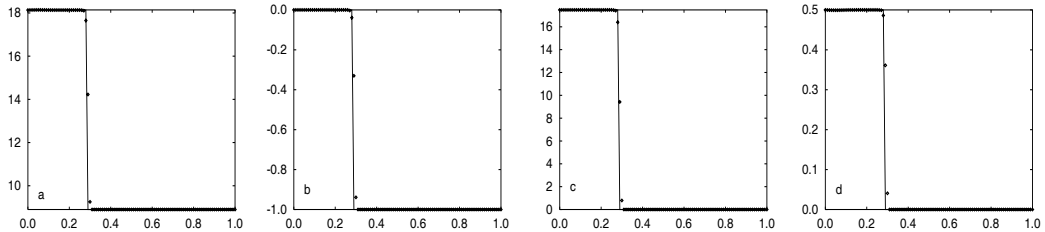

Figure 5: A shock reflection problem for stiffened equation of state (4.2) with $\gamma = 5/3$ and the pressure ratio $p^+/p^- \approx \infty$. The solutions at $t = 0.3$ are obtained with 100 points and $\Delta t = 0.0012$. (a) Density. (b) Velocity. (c) Pressure. (d) Internal energy.

The next problems we consider are two one-dimensional shock-tube problems with the initial data

$$(\rho, u, p)_{t=0} = \begin{cases} (19.13, 0, 17.5), & x < 0.5, \\ (8.9, 0., 2.013), & x > 0.5, \end{cases} \tag{4.3}$$

and

$$(\rho, u, p)_{t=0} = \begin{cases} (8.9, 0.3, 34.5), & x < 0.5, \\ (9.13, 0., 8.013), & x > 0.5, \end{cases} \tag{4.4}$$

for general EOS (4.2) with values for the parameters given in the previous.

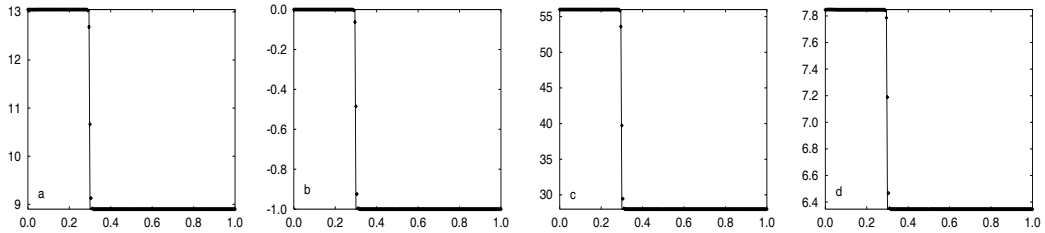

Figure 6: Same as Figure 5, except for the pressure ratio $p^+/p^- = 2$, $\Delta t = 0.0012$, 200 grid cells, and $t = 0.139$.

The numerical results (the dashed lines) shown in Figs. 7 and 8, are obtained with 200 points and a uniform time step. The exact solution involves a rarefaction wave, a contact discontinuity, and a shock wave.

From Figs. 7 and 8, we observe that strong shocks are resolved very well, but there is only slight numerical undershoot for velocity at contact discontinuity for problem (4.4).

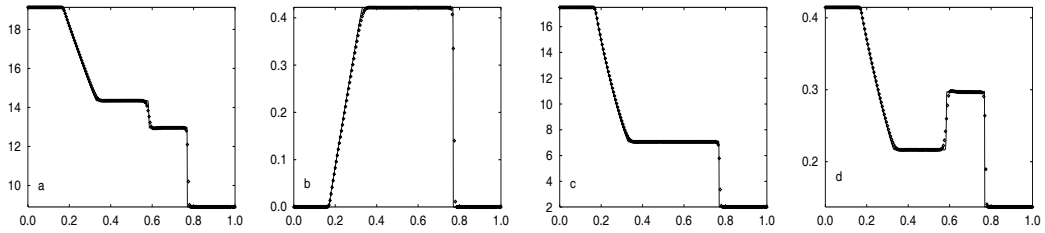

Figure 7: Shock–tube problem (4.3) for general equation of state (4.2). The solutions at $t = 0.2$ are obtained through high resolution KFVS schemes with 200 points (the dashed lines) and $\Delta t = 0.0017$. The solid lines are "exact solution" obtained with 2000 points. (a) density, (b) velocity, (c) pressure, (d) internal energy.

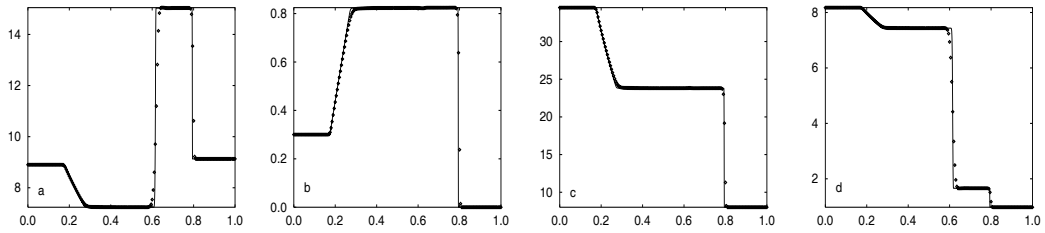

Figure 8: Same as Figure 8, except for shock–tube problem (4.4) and $t = 0.14$.

Before ending this section, we give computation of a two-dimensional test problem for dense gases, see [1, 19] for details, which is to study numerically reflections of planar shocks in dense gases from wedges. At first the simple planar shock meets the walls of the obstacle at left angles. The computational domain is 1×1, the right, upper and lower boundarys are considered as reflective (solid wall) boundary. At the left boundary, uniform post–shock states are used for the flow variables.

The problem considered here is the perfect gas limit of the van der Waals gas model. Initially, there is a shock with an incident shock Mach number M_I=1.65 at $x_0 = 0.1$, which propagates

in the x-direction. The post–shock states is taken as

$$(\rho, u_x, u_y, p) = (0.033, 5.016, 0.0, 3.001). \tag{4.5}$$

In this problem, we take $\delta = 0.4$ such that the initial condition is far from the thermodynamic critical point, and $\alpha = 20°$. The pre–shock states are decided according to the Ranking-Hugoniot jump conditions. Figs. 9 and 10 show the mass densities obtained by MUSCL type KFVS finite volume method and the time-accurate predictor-corrector TVD (PCTVD) scheme used in [2] with 150×150 grid resolution. Fig. 11 shows the mass densities obtained by MUSCL type KFVS finite volume method with 300×300 grid resolution. The slipstream in Figs. 9 and 11 has been resolved.

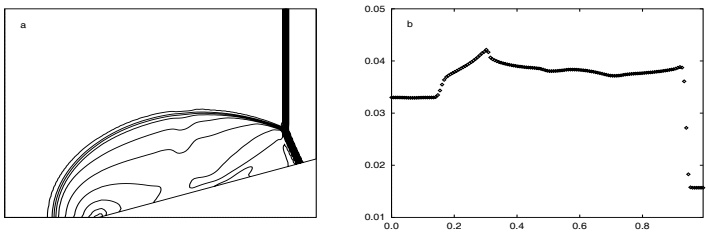

Figure 9: The density for two-dimensional problem obtained by using high resolution KFVS finite volume method with 150 × 150 grid cells. (a) Density distributions. (b) Density ρ profiles along the lower surface.

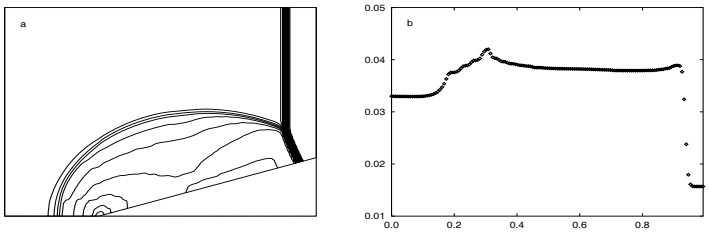

Figure 10: Same as Fig. 9 except for the PCTVD scheme in [1].

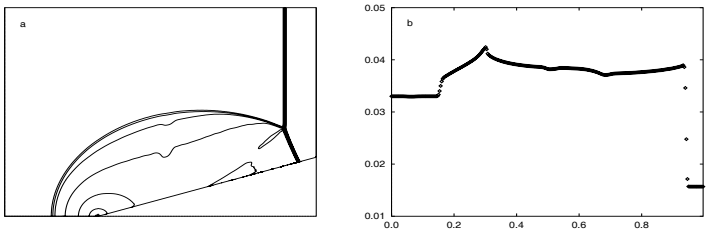

Figure 11: Same as Fig. 9 except for 300 × 300 grid cells.

5. Conclusion

In this paper we have introduced a distribution function $\bar{g}$ for the local equilibrium state to recover the Euler equations with a general pressure law, and presented a class of high resolution

MUSCL–type KFVS difference methods to approximate the Euler equations for real gases, which do not depend on the particular expression of the EOS and require derivatives of the pressure law. The similar idea of introducing an equilibrium distribution function can also be found in [14] for the γ–gas law.

The presented schemes have been applied to several test problems including a standard one dimensional shock reflection test problem and two shock-tube problems for three special equations of state. Numerical results show that the schemes (3.6) is of second order resolution at shock; they were well-resolved almost within two or three mesh interval. Moreover, the schemes gave correct location of discontinuities in comparison with the corresponding exact solutions. It is possible to improve further resolution of numerical solutions by combining the other higher order methods in space and time with KFVS to simulate numerically the Euler equations for real gases. These methods include higher order TVD Runge–Kutta time discretizations and WENO schemes etc. The current results are not restricted to several special equations of state. Extensions to multidimensional case is natural. They will be presented and compared in my forthcoming works.

Following the referees's comments, we may introduce a more physical local distribution function $\hat{g}$ that does not depend on the spatial dimensions. For one-dimensional flow problem, because both the fluid velocity components in y- and z-directions are considered as zero, we can define $\hat{g}$ as follows:

$$\widehat{g} = \rho(\frac{\lambda_1}{\pi})^{\frac{3}{2}}(\frac{\lambda_2}{\pi})^{\frac{K}{2}} e^{-\lambda_1(v_1-u)^2-\lambda_1(v_2^2+v_3^2)-\lambda_2\xi^2}, \tag{5.1}$$

with $K = \frac{5-3\gamma}{\gamma-1}$, and

$$\frac{\rho}{2\lambda_1} = p, \quad e = \frac{3}{4\lambda_1} + \frac{K}{4\lambda_2}. \tag{5.2}$$

In Fig. 12, we give the numerical solutions of a shock tube problem for a two-molecular vibrating gas with $\gamma = 1.4$, see [12], which are calculated by using two KFVS methods that are constructed based on $\bar{g}$ and $\hat{g}$, respectively. Two profiles of the density are essentially same. In Fig. 12, we also give distributions of two parameters γ_1 and γ_2 defined in (2.7) and (5.1), see the second and fourth picture, respectively. The results demonstrate our conclusion analyzed in Section 2 that both γ_1 and γ_2 are non-negative.

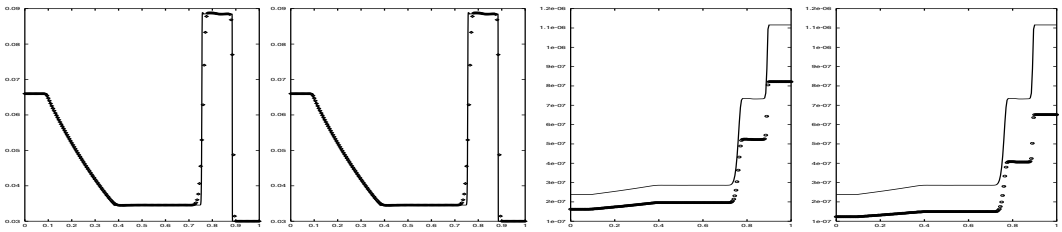

Figure 12: The solutions, ρ, γ_1 (solid line) and γ_2 (symbol), of a shock tube problem [12] for a two-molecular vibrating gas at $t = 2.5e-4$. Left: KFVS with $\bar{g}$; right: KFVS with $\hat{g}$.

References

[1] B.P. Brown and B.M. Argrow, Two-dimensional shock tube flow for dense gases, *J. Fluid Mech.* **349** (1997), 95-115.

[2] C. Cercignani: The Boltzmann Equation and its Applications, Springer-Verlag, 1988.

[3] S. Y. Chou and D. Baganoff, Kinetic flux-vector splitting for the Navier-Stokes equations, *J. Comput. Phys.*, **130** (1997), 217–230.

[4] S. Chapman and T.G. Cowling: The Mathematical Theory of Non-Uniform Gases, Third edition, Cambridge University Press, 1990.

[5] P. Colella and H.M. Glaz, Efficient solution algorithms for the Riemann problem for real gases, *J. Comput. Phys.*, **59** (1985), 264–289.

[6] F. Coquel and B. Perthame, Relaxation of energy and approximate Riemann solvers for general pressure laws in fluid dynamics equations, *SIAM J. Numer. Anal.*, **35** (1998), 2223–2249.

[7] P. Glaister, An approximate linearised Riemann solver for the Euler equations for real gases, *J. Comput. Phys.*, **74** (1988), 382–408.

[8] B. Grossman and R. W. Walters, Analysis of flux-split algorithms for Euler's equations with real gases, *AIAA J.*, **27** (1989), 524–531.

[9] M.S. Liou, B. van Leer, and J.S. Shuen, Splitting of inviscid fluxes for real gases, *J. Comput. Phys.*, **87** (1990), 1–24.

[10] A. Harten, B. Engquist, S. Osher and S. R. Chakravarthy, Uniformly high order accurate essentially non-oscillatory schemes, III, *J. Comput. Phys.*, **71** (1987), 231–303.

[11] J.C. Mandal and S.M. Deshpande, Kinetic flux vector splitting for Euler equations, *Computers and Fluids*, **23** (1994), 447–478.

[12] P. Montarnal and C. W. Shu, Real gas computation using an energy relaxation method and high–order WENO schemes, *J. Comput. Phys.*, **148** (1999), 59–80.

[13] J. M. Moschetta and D. I. Pullin, A robust low diffusive kinetic scheme for the Navier–Stokes /Euler equations, *J. Comput. Phys.*, **133** (1997), 193–204.

[14] B. Perthame, Second-order Boltzmann schemes for compressible Euler equations in one ant two space dimensions, *SIAM J. Numer. Anal.*, **29** (1992), 1–21.

[15] K.H. Prendergast and K. Xu, Numerical hydrodynamics from gas-kinetic theory, *J. Comput. Phys.*, **109** (1993), 53–66.

[16] D.I. Pullin, Direct simulation methods for compressible inviscid ideal gas flow, *J. Comput. Phys.*, **34** (1980), 231–244.

[17] K. S. Ravichandran, Higher order KFVS algorithms using compact upwind difference operators, *J. Comput. Phys.*, **130** (1997), 161–181.

[18] R.D. Reitz, One-dimensional compressible gas dynamics calculations using the Boltzmann equations, *J. Comput. Phys.*, **42** (1981), 108–123.

[19] H.Z. Tang, High resolution KFVS finite volume method for Euler equations for dense gases, preprint, ICM-99-08, Institute of Computational Mathematics, CAS, 1999.

[20] K. Xu, L. Martinelli, and A. Jameson, Gas–kinetic finite volume methods, flux-vector splitting and artificial diffusion, *J. Comput. Phys.*, **120** (1995), 48–65.

[21] B. van Leer, Towards the ultimate conservative difference schemes V. A second-order sequal to Godunov's method, *J. Comput. Phys.*, **32** (1979), 101–136.

[22] M. Vinokur and J.L. Montagne, Generalized flux-vector splitting and Roe average for an equilibrium for real gas, *J. Comput. Phys.*, **89** (1990), 276–300.